# Complexes of Alkylene-Linked Tacrine Dimers with *Torpedo californica* Acetylcholinesterase: Binding of Bis(5)-tacrine Produces a Dramatic Rearrangement in the Active-Site Gorge

Edwin H. Rydberg,[†,‡,§] Boris Brumshtein,[†,‡] Harry M. Greenblatt,[†] Dawn M. Wong,[†,‡] David Shaya,[†,‡] Larry D. Williams,[∥] Paul R. Carlier,[∥] Yuan-Ping Pang,[⊥] Israel Silman,[‡] and Joel L. Sussman*[,†]

*Departments of Structural Biology and Neurobiology, Weizmann Institute of Science, Rehovot 76100, Israel, Instituto di Ricerche di Biologia Molecolare P. Angeletti, Pomezia (RM) 00040, Italy, Department of Chemistry, Virginia Tech, Blacksburg, Virginia 24061, and Computer-Aided Molecular Design Laboratory, Mayo Clinic College of Medicine, Rochester, Minnesota 55905.*

*Received February 14, 2006*

The X-ray crystal structures were solved for complexes with *Torpedo californica* acetylcholinesterase of two bivalent tacrine derivative compounds in which the two tacrine rings were separated by 5- and 7-carbon spacers. The derivative with the 7-carbon spacer spans the length of the active-site gorge, making sandwich interactions with aromatic residues both in the catalytic anionic site (Trp84 and Phe330) at the bottom of the gorge and at the peripheral anionic site near its mouth (Tyr70 and Trp279). The derivative with the 5-carbon spacer interacts in a similar manner at the bottom of the gorge, but the shorter tether precludes a sandwich interaction at the peripheral anionic site. Although the upper tacrine group does interact with Trp279, it displaces the phenyl residue of Phe331, thus causing a major rearrangement in the Trp279-Ser291 loop. The ability of this inhibitor to induce large-scale structural changes in the active-site gorge of acetylcholinesterase has significant implications for structure-based drug design because such conformational changes in the target enzyme are difficult to predict and to model.

## Introduction

The adverse effects of anticholinergic drugs on memory,[1] taken together with postmortem data that revealed low levels of cholinergic markers in patients with Alzheimer's disease (AD),[2] led to the cholinergic hypothesis, which postulates that AD is associated with impairment of cholinergic transmission.[3,4] It was, therefore, suggested that inhibition of acetylcholinesterase (AChE), the enzyme responsible for the termination of synaptic transmission by rapid hydrolysis of the neurotransmitter acetylcholine (ACh), might provide symptomatic relief, at least for early-stage AD patients. Indeed, all of the first-generation drugs approved for the management of AD were cholinesterase inhibitors (ChEIs).[5,6] Butyrylcholinesterase (BuChE) is an enzyme with high structural homology to AChE.[7] Despite its wide tissue distribution, its precise biological function remains to be established.[7] However, whereas AChE levels in the brains of AD patients are reduced, levels of BuChE are elevated.[8] Indeed, there is evidence that inhibition of BuChE may also be advantageous in the treatment of AD patients.[9,10] It has been demonstrated that AChE can accelerate the assembly of A$\beta$ to the amyloid fibrils, which are associated with plaque deposition in AD patients,[11−13] and that the functional site in this process is the peripheral anionic site (PAS) at the entrance to the active-site gorge. Indeed, the capacity of intact AChE to promote A$\beta$ assembly can be mimicked by a hydrophobic peptide, part of whose sequence corresponds to the PAS of *Torpedo californica* AChE (*Tc*AChE).[14]

Thus, the design of second-generation ChEIs for the treatment of AD should take into account not only the possible interaction with other targets, for example, nicotinic[15] or glutamatergic[16] receptors, but also the selectivity for AChE versus BuChE or for the PAS of AChE versus its catalytic anionic subsite (CAS). It may, in principle, be desirable to design inhibitors with either broad specificity for all three targets or narrow specificity for only one of them. Recent articles have indeed described the synthesis of selective inhibitors in this context.[17−20] The use of ChEIs is also being explored for the treatment of other dementias and other neurological indications.[9] The same considerations mentioned above in selecting a ChEI-type drug for the treatment of AD should also be applied in selecting one for the treatment of these other clinical targets.

The bivalent ligand strategy involves the synthesis of drugs in which identical or different pharmacophores are linked via a suitable linker. This strategy takes advantage of the chelate effect[21] to create a bifunctional ligand with enhanced affinity for its target. The geometry of the active-site gorge of AChE, with specific sites at its two extremities,[22,23] makes it a particularly suitable target for applying this approach. Even before the 3D structure of AChE was known, bivalent ligands, such as decamethonium,[24] BW284C51,[25] and ambenonium[26] were described, which displayed both high affinity and high selectivity for this enzyme. Recent examples of successful utilization of this strategy include **2f**,[27] the triazole-linked phenylphenanthridium-based inhibitor, *syn*-TZ2PA6, which displays a 77 fM binding constant for *Tc*AChE,[28] and a more potent triazole analogue with a dissociation constant of 33 fM for eel AChE.[29] The development of bivalent AChE inhibitors as potential therapeutic drugs for AD has been recently reviewed.[30] An important observation made in applying this strategy to AChE was that pharmacophores with weak affinities for AChE can serve as effective PAS-directed ligands when incorporated into a bivalent drug.[31] Thus, in principle, one can design bivalent drugs, which, by spanning the active-site gorge, can inhibit the physiological actions of both the catalytic and peripheral sites. Furthermore, because aromatic residues, which are the principal elements of the PAS in vertebrate AChEs, are

* Corresponding author. Phone: 972-8-934-4531. Fax: 972-8-934-4159. E-mail: joel.sussman@weizmann.ac.il.
† Department of Structural Biology, Weizmann Institute of Science.
‡ Department of Neurobiology, Weizmann Institute of Science.
§ Instituto di Ricerche di Biologia Molecolare P. Angeletti.
∥ Virginia Tech.
⊥ Mayo Clinic College of Medicine.

10.1021/jm060164b CCC: $33.50 
Published on Web 08/09/2006

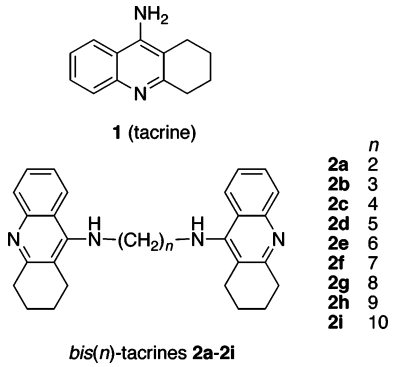


**Figure 1.** Structures of tacrine and bis(n)-tacrine derivatives.

**Table 1.** Inhibition and Selectivity of Tacrine and Bis-tacrine Compounds Acting on Rat AChE and BuChE (from ref 37)[a]

| compd | rat brain AChE $IC_{50}$ (nM) | rat serum BuChE $IC_{50}$ (nM) | selectivity[b] for AChE |
|---|---|---|---|
| tacrine | 223 ± 11 | 92 ± 2 | 0.40 |
| **2a** | 711 ± 25 | 102 ± 4 | 0.14 |
| **2b** | 254 ± 55 | 152 ± 17 | 0.60 |
| **2c** | 157 ± 23 | 252 ± 9 | 1.60 |
| **2d** | 28 ± 5 | 329 ± 21 | 11.7 |
| **2e** | 3.8 ± 0.4 | 119 ± 6 | 31.6 |
| **2f** | 1.5 ± 0.3 | 149 ± 23 | 99.4 |
| **2g** | 7.8 ± 0.9 | 105 ± 13 | 13.5 |
| **2h** | 31 ± 3 | 155 ± 25 | 4.9 |
| **2i** | 40 ± 6 | 167 ± 12 | 4.2 |

[a] The 7-methylene linker results in the optimal spacing between tacrine moieties.[27,37] [b] Selectivity is defined as BuChE($IC_{50}$)/AChE($IC_{50}$).

lacking in the homologous BuChEs,[7,32] one can design bivalent ligands with high selectivity for AChE relative to that for BuChE.

Tacrine, as Cognex, was the first ChEI approved by the FDA for the management of AD.[33] It has, however, been replaced by other ChEIs because of its hepatoxicity.[34] Computational studies[35] suggested that tacrine interacts with AChE, not only at the CAS, principally through a stacking interaction with Trp84,[36] but also, with lower affinity, by interaction with the indole ring of Trp279 at the PAS. It was thus predicted that bis-tacrines in which the two pharmacophores were separated by a linker of a suitable length would have both greater inhibitory potency and selectivity than tacrine itself, a hypothesis that was confirmed via the synthesis and testing of a series of bis-(n)-tacrine congeners (Figure 1, Table 1).[27,37] One of these compounds, heptylene-linked bis-tacrine, (**2f**), was indeed 150-fold more active against rat AChE than tacrine and up to 250-fold more selective for AChE than for BuChE.[37] Pentylene-linked bis-tacrine (**2d**) was less potent and selective than **2f** but was, nevertheless, an order of magnitude more potent and more selective than tacrine itself.[37]

In the following, we present and analyze the crystal structures of the complexes of **2d** and **2f** with *Tc*AChE, viz. **2d**/*Tc*AChE and **2f**/*Tc*AChE, respectively. We show that the interactions of **2d** with both the CAS and the PAS involve a drastic rearrangement of the protein structure, especially in the vicinity of the acyl binding pocket, whereas the binding of **2f** can be accommodated with changes in the conformations of two side-chains in the active-site gorge.

The structures of the two complexes, namely **2d**/*Tc*AChE and **2f**/*Tc*AChE, have been submitted to the Protein Data Bank (PDB), with accession codes of 2cmf and 2ckm, respectively.

**Table 2.** Data Collection Parameters and Processing Statistics

| | **2d** | **2f** |
|---|---|---|
| space group | $P3_121$ | $P3_121$ |
| wavelength (Å) | 0.933 | 1.514 |
| oscillation angle (deg), exposure time (sec) | 0.5, 7 | 0.5, 1200 |
| total number of frames | 60 | 98 |
| total number of reflections | 179411 | 419866 |
| unique reflections | 34365 | 50434 |
| overall redundancy | 1.8 | 2.9 |
| mosaicity (degrees) | 0.53 | 0.43 |
| resolution range (Å) | 30−2.5 | 30−2.15 |
| overall completeness | 96.6% | 92.3% |
| completeness in highest resolution shell | 96.7% | 75.6% |
| overall $R_{merge}$ | 5.0% | 4.7% |
| $R_{merge}$ in highest resolution shell | 39.5% | 51% |

## Materials and Methods

**Crystallization and Data Collection.** *Tc*AChE was purified and crystallized as described.[22] Inhibitors **2d** and **2f** were synthesized and characterized as previously reported.[37]

Soaking solutions were prepared by dissolving **2d** and **2f** in 40% PEG200 (v/v)/0.1 M MES buffer at pH 5.8, at concentrations of 2 and 0.5 mM, respectively. Trigonal *Tc*AChE crystals were transferred to 6 $\mu$L drops of soaking solution at 4 °C and left overnight. The crystals were then transferred to oil, mounted on a nylon loop, and flash cooled in an Oxford Cryosystems cryostream.

Data collection for the **2f**/*Tc*AChE complex was performed at the Weizmann Institute, using a RIGAKU RU-H3R running at 50 kV/100 mA with Osmic blue confocal optics at 120 K. Diffraction images were recorded on a RAXIS-IV$^{++}$ (100 $\mu$ mode). Two crystals were used, and the data from both were combined into a unified set. Data for the **2d**/*Tc*AChE complex were collected at the ESRF synchrotron in Grenoble, on beamline ID14-2 at 100 K, with an ADSC Quantum4 CCD detector. In both cases, the program STRATEGY[38] was used to identify the optimal data collection protocol. DENZO and SCALEPACK[39] were used to integrate and scale the data. Final data collection results are summarized in Table 2. Data were truncated with the CCP4[40] program TRUNCATE,[41] and a list of randomly generated test reflections was added from a master list for the trigonal crystal form of *Tc*AChE using CAD and FREERFLAG.[42] Reflections were output with MTZ2VARIOUS to a format suitable for CNS.

**Structure Determination and Refinement for the 2f/*Tc*AChE Complex.** The initial model for structure determination was taken from previous examples of the trigonal crystal form of *Tc*AChE (based on PDB code 2ace) without solvent molecules, and carbohydrate residues. Rigid body refinement (CNS[43]) was used to check the handedness of the data and to account for slight deviations in cell constants. Initial electron density maps (2*F*o-*F*c and *F*o-*F*c) were calculated, and the initial *F*o-*F*c map was used to fit two tacrine moieties to the density observed in the gorge, using the Xfit program.[44] However, because no electron density was observed for the 7-carbon alkyl linker, it was removed from the model. The side chains of Trp279 and Phe330 were adjusted to move them from negative electron density peaks to nearby positive electron density peaks. Simulated annealing[45] was performed for *Tc*AChE with the partial inhibitor model, followed by individual B-factor refinement. At this stage, $R_{work}$ was 23.5%, and $R_{free}$ was 27.2%.

As the map phases improved with subsequent refinement, the linker chain was gradually built into the ligand electron density, and water molecules were added. Refinement progressed until convergence of $R_{free}$. For the final refinement step, occupancy for the ligand was set to 0.9 because of negative

**Table 3.** Refinement Results

| | 2d | 2f |
|---|---|---|
| resolution range (Å) | 30.0−2.5 | 30−2.15 |
| number of protein atoms | 4165 | 4142 |
| number of non protein atoms | 171 | 272 |
| solvent (water) molecules | 108 | 207 |
| carbohydrate atoms | 28 | 28 |
| inhibitor atoms | 35 | 37 |
| $R_{work}$ (%) | 21.3 | 21.1 |
| $R_{free}$ (%) | 25.7 | 24.9 |
| rms bond deviation | 0.015 Å | 0.0127 Å |
| rms angle deviation | 1.18° | 1.65° |
| protein main-chain average B-factor | 66.5 | 43.0 |
| protein side-chain average B-factor | 66.8 | 43.6 |
| carbohydrate average B-factor | 85.9 | 66.0 |
| water molecules average B-factor | 65.3 | 47.7 |
| ligand average B-factor | 59.3 | 49.0 |

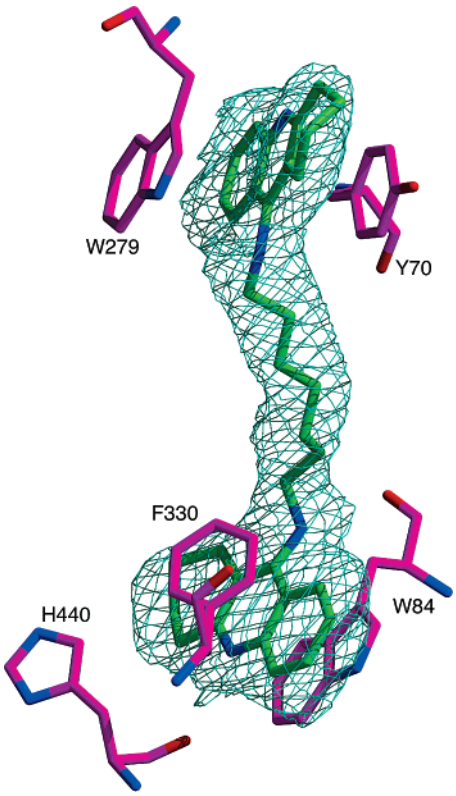


**Figure 2.** Simulated annealing omit difference map in the region of the active site for the **2f**/*Tc*AChE complex. **2f** is rendered with green carbon atoms, and protein residues with magenta carbon atoms. Contouring is at 3.0$\sigma$, within a radius of 2.0 Å of the inhibitor atoms. The Figure was created using Xfit[44] and Raster3D.[46]

density (−4$\sigma$) for the tacrine bound at the PAS. Peak searches for water molecules were performed, with particular attention being paid to the region of the active site. Upon completion of refinement, 207 water molecules had been added. Final refinement results are summarized in Table 3.

Finally, a simulated annealing omit map was calculated, excluding all atoms within a radius of 3.5 Å around the ligand (Figure 2).

**Structure Determination and Refinement for the 2d/*Tc*AChE Complex.** The starting *Tc*AChE model was the same as that used for the **2f** complex. Rigid body refinement (CNS) was used to check the handedness of the data and to account for slight deviations in cell constants. Initial maps ($F_o$-$F_c$ and $2F_o$-$F_c$) showed unambiguous density for the inhibitor, allowing placement of both tacrine moieties and the linker group, making use of the XtalView program.[44] As refinement progressed, two carbohydrate moieties and 108 water molecules were fitted. The inhibitor molecule was refined at full occupancy.

The initial difference map indicated a change in the conformation of the loop from Phe284 to Arg289 relative to its conformation in native *Tc*AChE. These residues were, therefore, removed from the model during the early rounds of refinement and refitted in stages as refinement progressed.

At the end of refinement, a composite omit map was calculated for the entire structure. The inhibitor is shown in Figure 3a, and the region of the Phe284-Ser291 loop is shown in Figure 3b.

## Results

**2f/*Tc*AChE Complex.** The proximal tacrine ring of **2f** is bound at the CAS, sandwiched between Trp84 and Phe330, very similarly to that in the tacrine/*Tc*AChE structure (PDB code 1acj).[36] No significant conformational changes in the residues of the catalytic triad were detected, and the water molecule observed in the native structure near the catalytic Ser200 is retained.

The heptylene linker spans the aromatic gorge, connecting the tacrine rings bound at the PAS and CAS. No changes in the conformation of side chains lining the mid-portion of the gorge are observed relative to the native structure (Figure 4).

The peripheral tacrine ring is bound at the PAS by stacking between Tyr70 and Trp279. For this interaction to occur, the side chain of Trp279 undergoes an ∼60° rotation about $\chi_1$, and an ∼224° rotation about $\chi_2$, relative to its conformation in native *Tc*AChE (Figure 4).

**2d/*Tc*AChE Complex.** The proximal ring of **2d** is bound in the CAS similarly to the way it is bound both in tacrine/*Tc*AChE and **2f**/*Tc*AChE. However, the distance between Ser200-$O^{\gamma}$ and H440-$N^{\epsilon 2}$ is 3.7 Å compared to 2.6 Å in **2f**/*Tc*AChE, 2.7 Å in native *Tc*AChE (PDB code 2ace), and 3.3 Å in tacrine/*Tc*AChE (PDB code 1acj). Thus, the catalytic triad is disrupted.

In **2d**/*Tc*AChE, the main-chain atoms of Phe331 are displaced 1 Å toward the opening of the gorge, with respect to native *Tc*AChE, presumably to alleviate the potential steric clash of its side chain with the distal tacrine moiety. The resultant 1.9 Å shift in the position of the phenyl ring of Phe331 appears, in turn, to produce an unfavorable steric contact with the side chain of Phe288. The alleviation of this clash has dramatic consequences, as discussed in the next section.

In **2d**/*Tc*AChE, the distal tacrine moiety is stacked against the indole of Trp279. Interestingly, this interaction with Trp279 leaves the side-chain of this residue in its native conformation (Figure 5), differing from its conformation in both the tacrine/*Tc*AChE and **2f**/*Tc*AChE structures.

The largest structural alterations, upon the binding of **2d** to *Tc*AChE, are observed in the Trp279-Ser291 loop,[48] which bears residues of both the acyl pocket and the PAS. The backbone atoms in this region are displaced as much as 4.7 Å (Asp285-$C^{\alpha}$) from their native positions, and the side-chains of Phe284, Phe288, and Phe290 are dramatically reoriented. The 1 Å movement of Phe331, induced by **2d** (see above), results in a disruption of its stacking interaction with Phe288. To avoid steric clashes with Trp233 and Asn399, the $C^{\alpha}$ of Phe288 moves 1.9 Å, and the side-chain is rotated ∼70° about $\chi_1$ (Figure 6). To accommodate these movements, the main chain from Trp279 to Phe290 adopts a drastically altered conformation. At the distal end of the loop, Phe290 $C^{\alpha}$ moves 0.6 Å, with a concomitant 180° rotation of the side-chain about $\chi_1$ and the formation of an edge-face interaction with the indole ring of Trp279.

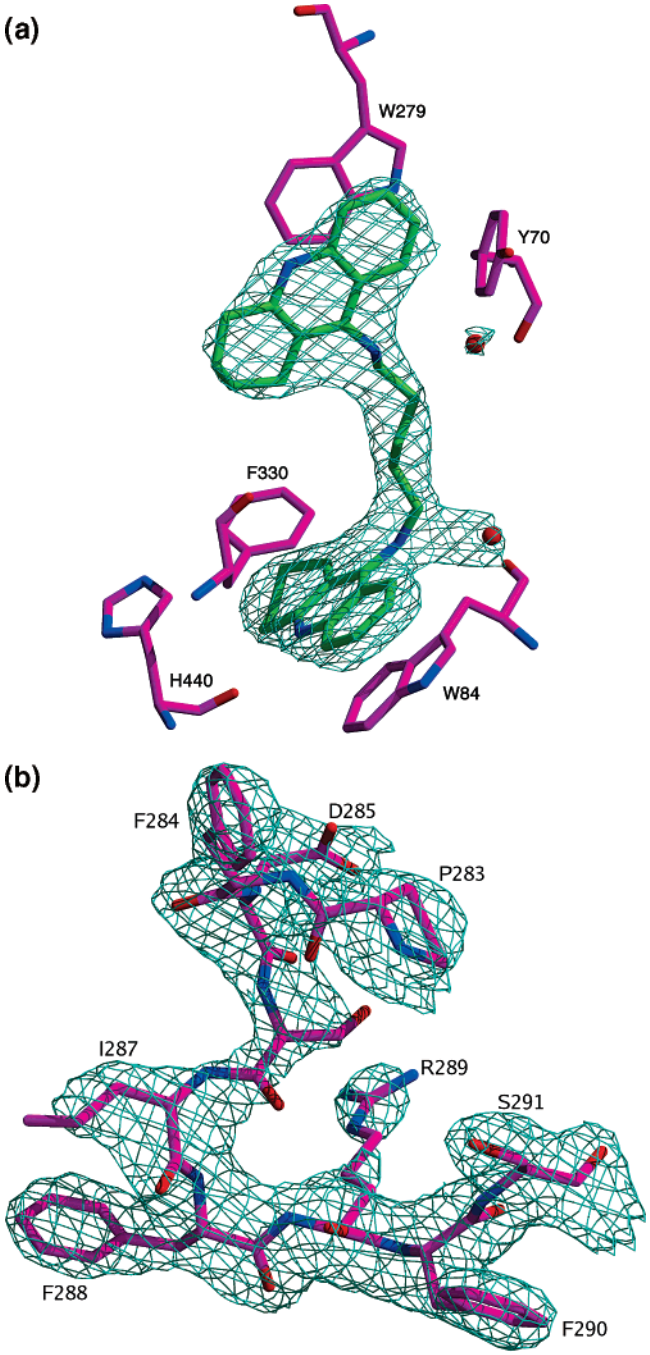


**Figure 3.** (a) Simulated annealing composite omit map of the **2d**/*Tc*AChE complex. The inhibitor carbon atoms are colored green, whereas those of the protein are magenta. Two water molecules are shown as red spheres. Contouring is at 1.3$\sigma$, within a radius of 2.0 Å around the inhibitor atoms and water molecules. (b) Simulated annealing composite omit map for residues Pro283−Ser291, overlayed with the final refined model. Contouring is at 1.3$\sigma$, at a radius of 2.0 Å from each atom in the loop. The Figure was created using the same graphics programs used for Figure 2.

The effect of this rearrangement on the surface of the active-site gorge is shown in Figure 7. The movement of Phe288 and Phe290 expands the volume of the acyl binding pocket, as can be seen in the lower part of the 3rd panel in Figure 7a and in the side view in Figure 7b compared to the corresponding views for the native enzyme in the upper panels in both figures and for **2f**/*Tc*AChE, in the corresponding middle panels.

The rearrangement of the Trp279-Phe290 loop also results in movements in the more distal parts of the *Tc*AChE molecule (Figure 8). Thus, the backbone atoms between Lys325 and Phe339, between Ile347 and Asn383 (which includes two helices), and from Leu516 to Thr535 (*C*-terminal) are all substantially shifted from their positions in the native structure. It should be noted that the second helix in the Ile347−Asn383 segment and that in the *C*-terminal segment are both part of the four-helix bundle involved in dimer formation.

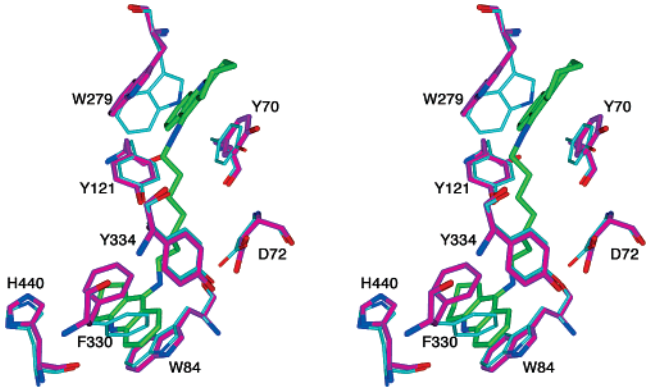


**Figure 4.** Comparison of the native conformations (cyan carbon atoms) of selected residues in the active-site gorge of *Tc*AChE with their corresponding conformations in the **2f**/*Tc*AChE complex (magenta carbon atoms). The inhibitor is rendered with green carbon atoms. The Figure was created with PyMOL.[47]

## Discussion

**Increased Potency and Selectivity of 2f Results from the Binding of the Distal Tacrine Ring at the PAS.** The observed increase in potency (150-fold) and selectivity (250-fold with respect to BuChE) of **2f** over tacrine[37] can clearly be ascribed to the interaction of its distal tacrine with both Trp279 and Tyr70 at the PAS of *Tc*AChE. The nature of this interaction, assuming the distal tacrine ring is protonated, would be both a cation-$\pi$ and a $\pi-\pi$ stacking interaction. The $\pi-\pi$ stacking interactions are estimated to provide ~2 kcal/mol of binding energy (see, for example, Boehr et al., 2002[50]), equivalent to a ~50-fold change in $IC_{50}$. Hydrophobic interactions of the linker with gorge residues and entropy gained in displacing gorge-bound water molecules may also contribute to the enhanced affinity, although this will be offset somewhat by the loss of entropic freedom of the linker group. Moreover, the presence of the two binding moieties greatly increases the selectivity for AChE over BuChE because the latter does not possess a PAS. Somewhat longer bis(n)-tacrines (e.g., with linker groups of 8 or 9 carbon atoms) might be expected to make interactions similar to those made by **2f**. This was indeed shown in a recent study that reported the crystal structure of the complex of *Tc*AChE with NF595, a close homologue of **2f** containing an 8-carbon spacer.[51] But the longer linkers are likely to pay larger entropic costs when binding in the gorge. Thus, our analysis of the structural basis for both the binding mode and increased efficacy of **2f** compared to those of tacrine supports the hypothesis generated by the original computational analysis[27] and rationalizes the optimal binding of **2f**.

**Disruption of the Catalytic Triad in 2d/*Tc*AChE.** Interestingly, although the binding of the tacrine moiety to the catalytic site appears to be similar in the three structures solved (complexes of tacrine, **2d**, and **2f** with *Tc*AChE), there are significant differences in the position of the catalytic Ser200. While Ser200 $O^{\gamma}$ interacts with His440 $N^{\epsilon 2}$ in three structures, (native *Tc*AChE = 2.7 Å, tacrine/*Tc*AChE = 3.3 Å, **2f**/*Tc*AChE = 2.6 Å), the binding of **2d** appears to disrupt this interaction such that this distance becomes 3.7 Å. Ser200 $O^{\gamma}$, in fact, is

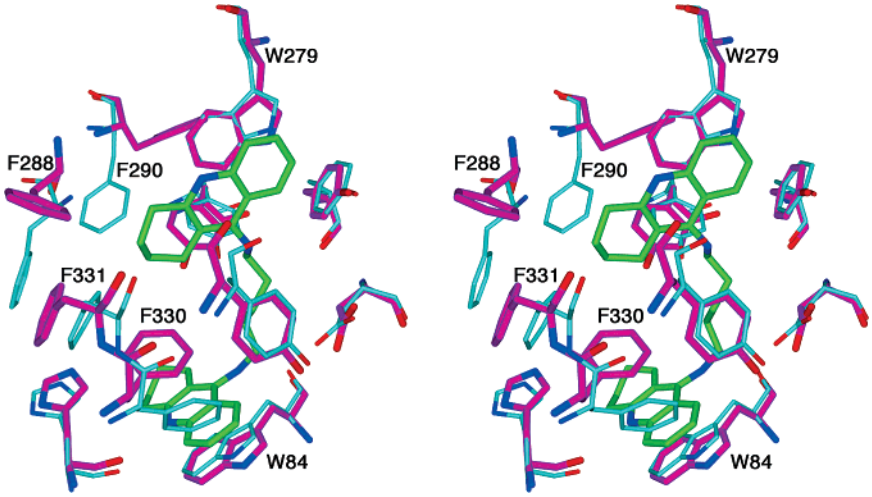


**Figure 5.** Comparison of the native conformations (cyan carbon atoms) of selected residues in the active-site gorge of *Tc*AChE with their corresponding conformations in the **2d**/*Tc*AChE complex (magenta carbon atoms). The inhibitor is rendered with green carbon atoms. The model of the native structure was taken from the results of the initial rigid body refinement. The Figure was created with PyMOL.[47]

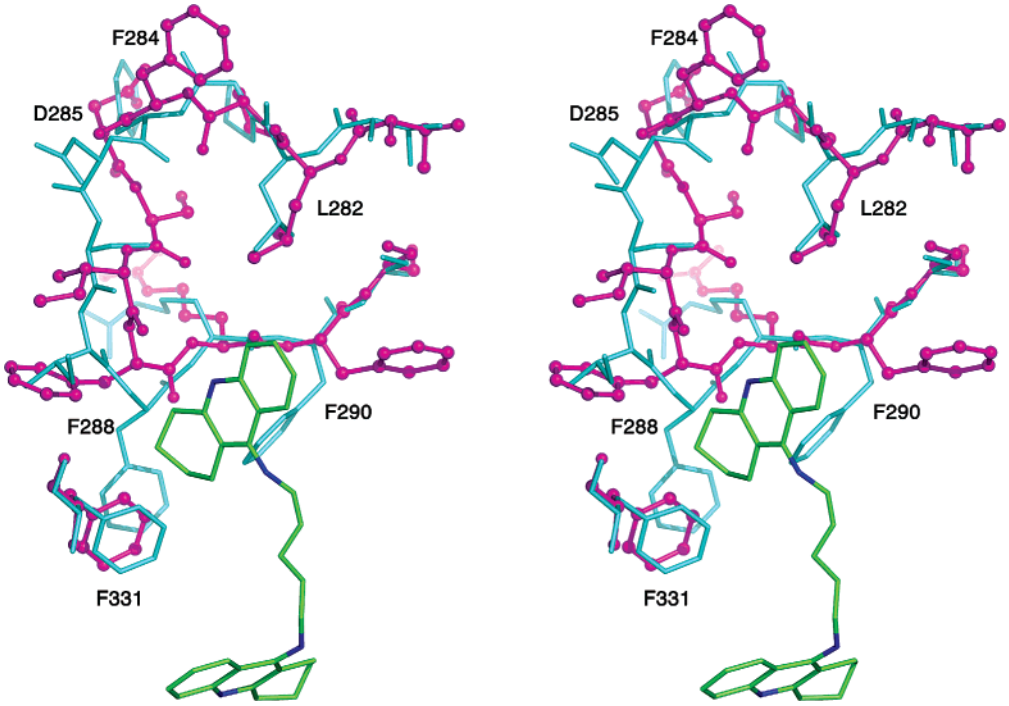


**Figure 6.** Stereoview of the Val281−Ser291 segment in native *Tc*AChE (cyan) and **2d**/*Tc*AChE (magenta atoms for the protein and green carbon atoms for the inhibitor). The Figure was created with PyMOL.[47]

shifted towards the oxyanion hole, interacting with the main-chain nitrogen atoms of Ala201 (2.8 Å), Gly118 (3.3 Å), and Gly119 (3.5 Å), which are not noticeably displaced from their native positions.

**Binding of 2d to *Tc*AChE Induces Unique Reorientations in the Active-Site Gorge.** Despite the drastic rearrangements caused by the binding of **2d**, the inhibitor was, nevertheless, shown to be 8-fold more potent and 30-fold more selective than tacrine in rat AChE.[37] Presumably, the energetics of the $\pi-\pi$ stacking between **2d** and Trp279 and the newly formed edge−face interaction between Phe290 and Trp279 are strong enough to overcome the energy barrier involved in reorientation.

Only two previous examples of significant movement of the acyl-binding loop have been observed in AChE crystal structures, both of which differ from that seen in the **2d**/*Tc*AChE complex. In the conjugate produced by the interaction of the organophosphate, diisopropylphosphorofluoridate (DFP) with *Tc*AChE, the crystal structure (PDB code 2dfp) shows that the isopropyl group of the covalently attached organophosphoryl moiety, which resides in the acyl binding pocket, clashes with the phenyl rings of Phe288 and Phe290. This results in the displacement of the backbone atoms of the acyl pocket by almost 5 Å,[52] although the phenyl rings of both Phe288 and Phe290 maintain orientations similar to those that they assume in the native structure. There is, however, a substantial reorientation of the side chain of Arg289, whose $C^{\alpha}$ is displaced by 4.8 Å. Recently, the crystal structure of the complex of 9-dehydro-6-*O*-demethyl-6-*O*-(8′-phthalimidooctyl)-galanthamine with *Tc*AChE (PDB code 1w76) has been elucidated.[53] The galanthamine moiety of the ligand is positioned just like native galanthamine in its complex with *Tc*AChE.[54] Consequently, the bulky phthalimido group is oriented towards the acyl binding pocket, and produces disorder in the Asp285-Phe288 loop, demonstrating the high degree of flexibility of this loop and showing a

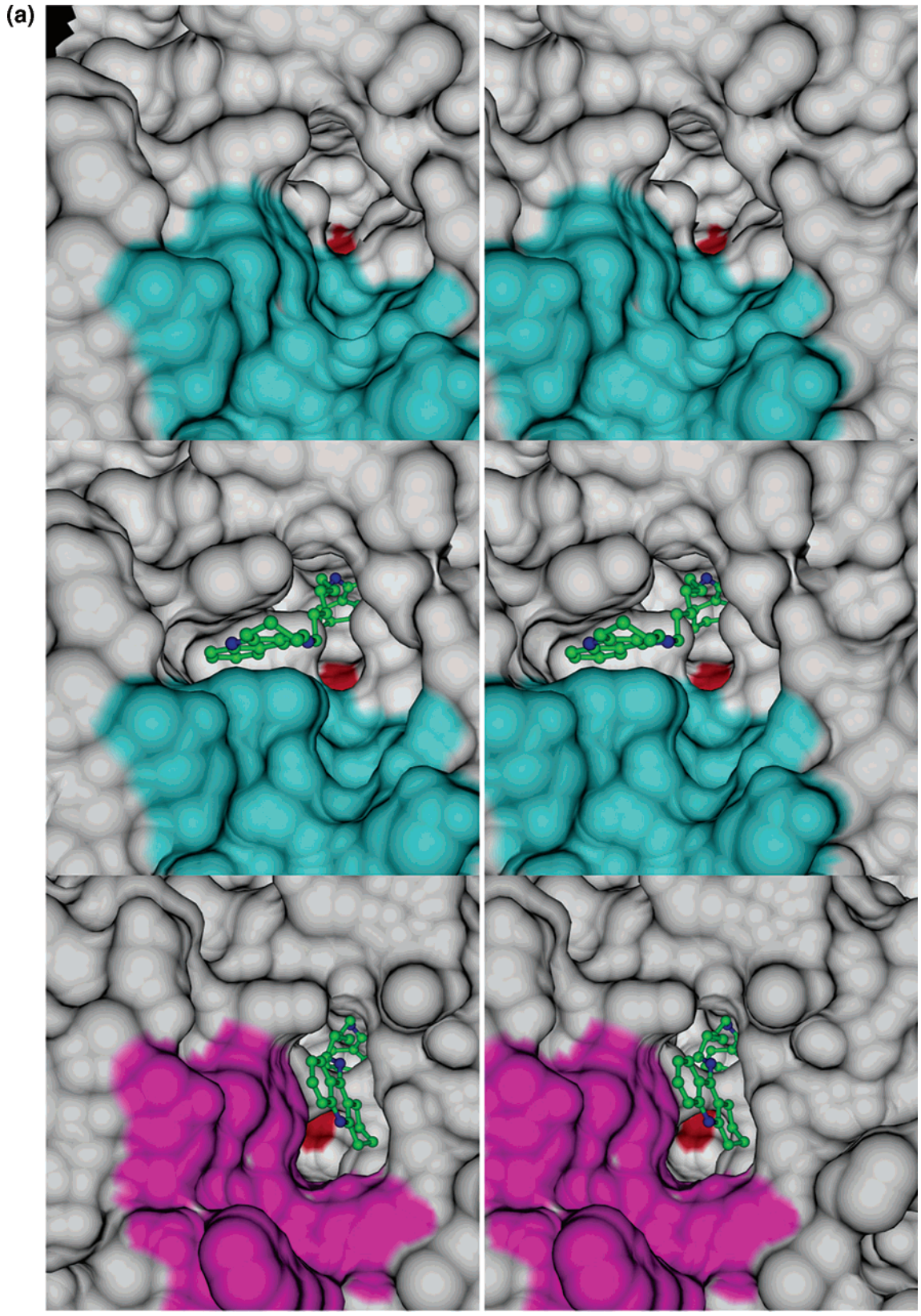


**Figure 7.** (a) Stereoviews looking down the gorge of *Tc*AChE. The red color is the surface associated with Ser200 $O^{\gamma}$. The top panel shows the surface for the native enzyme, the middle panel shows the corresponding surface for **2f**/*Tc*AChE, and the lower panel for **2d**/*Tc*AChE. The surface associated with the loop Trp279-Ser290 is colored cyan in the native structure and in **2f**/*Tc*AChE and magenta in **2d**/*Tc*AChE. The Figure was created with DINO,[49] and rendered in POV-Ray. (b) Stereo side-view of gorge in native *Tc*AChE (top panel), **2f**/*Tc*AChE (middle panel), and **2d**/*Tc*AChE (bottom panel). This orientation is rotated roughly 90° relative to Figure 7a and represents the view from the right side of Figure 7a. The coloring of the enzyme surface is the same as that in Figure 7a. The carbon atoms of the enzyme are colored salmon and those of the inhibitor are green. The expanded region of the acyl binding pocket is visible in the **2d** complex. The Figure was created using the same process as for Figure 7a.

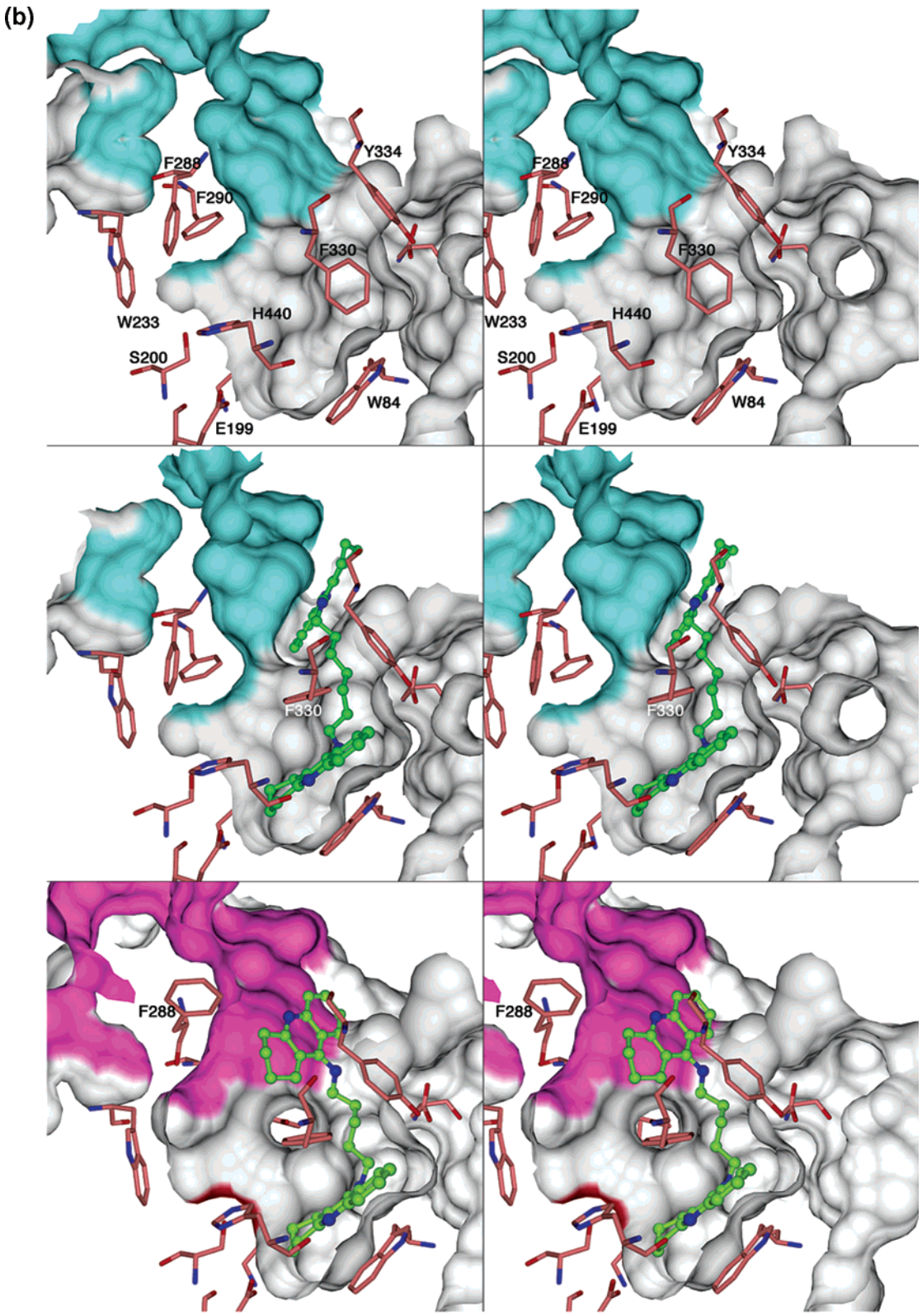


**Figure 7. (cont.)**

possible pathway from the active site to the bulk solvent. Thus, the three crystal structures, taken together, provide evidence for the ability of the acyl binding loop to adopt multiple conformations of varying stability and suggest that its role in catalysis by AChE is worthy of more detailed study.

Another example of inhibitor-induced movement involves the complex between mouse AChE and the *syn*-isomer of the gorge-spanning ligand, TZ2PA6 (PDB code 1q83), prepared by *in situ* click chemistry.[28] In this case, the linker between the tacrine moiety at the bottom of the gorge and the phenathridinium group near its mouth pull the distal group downward, producing an unanticipated conformational change.[55] In the complex, the indole group of Trp286 (homologous to Trp279 in *Tc*AChE) is dislodged from its native position, forming a sandwich type interaction with the phenanthridinium moiety and Tyr72 (homologous to Tyr70 in *Tc*AChE), although with the opposite face of the indole ring, relative to the **2f**/*Tc*AChE structure. In addition, the main-chain atoms of the dipeptide Tyr341-Gly342

**Table 4.** Comparison of Exocyclic Dihedral Angles (as defined in Figure 9) of Various Tacrine-Derived Inhibitors (Figure 10) in Complex with AChE[a]

| tacrine-containing ligand | PDB code | source organism of AChE | dihedral angle (deg) | associated energetic penalty for **4** (B3LYP/6-31G*, kcal/mol) |
|---|---|---|---|---|
| **2d** | 2cmf | *Torpedo californica* | 135(CAS)<br>73 (PAS) | 1.5<br>7.2 |
| **2f** | 2ckm | *Torpedo californica* | 68 (CAS)<br>−169 (PAS) | 7.2<br>0.0 |
| **6** | 1odc[b] | *Torpedo californica* | 81 | 8.3 |
| **7** | 1ut6[b] | *Torpedo californica* | 89 | 9.0 |
| (*R*)-**8** | 1zgb[c] | *Torpedo californica* (trigonal) | 113 | 5.5 |
| (±)-**8** | 1zgc[c,d] | *Torpedo californica* (orthorhombic) | 45, 62 | 4.5, 5.6 |
| *syn*-TZ2PA6 | 1q83[d] | *Mus musculus* | 132, 127 | 2.7 |
| *anti*-TZ2PA6 | 1q84[d] | *Mus musculus* | 47, 35 | 4.5, 3.8 |

[a] The complexes of ligands **6** and **7** both feature near orthogonal dihedral angles that would create a significant energetic penalty in protonated *N*-methyltacrine **4**. The complexes of ligand **8**, *syn*- and *anti*-TZ2PA6 possess dihedrals approaching a 45° deviation from co-planarity with the tacrine unit, thereby incurring a lower energetic cost. [b] Wong, D. M., Brumsthein, B., Greenblatt, H. M., Carlier, P. R., Han, Y.-F., Pang, Y.-P., Silman, I., Sussman, J. L. Unpublished results. [c] Haviv et al., 2005.[58] [d] The crystal form has two molecules in the asymmetric unit; the values are given for each.

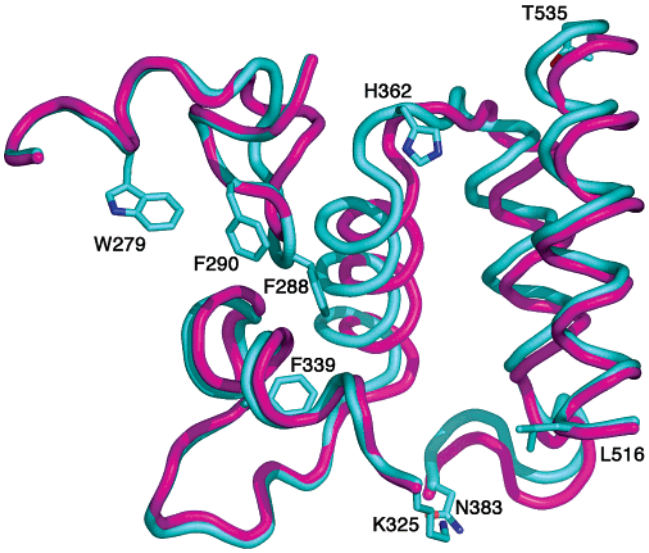


**Figure 8.** Cα trace of regions affected by the binding of **2d** to *Tc*AChE. The native structure, with selected side-chains, is shown in cyan, and the structure of the complex is shown in magenta. The Figure was created with PyMOL.[47]

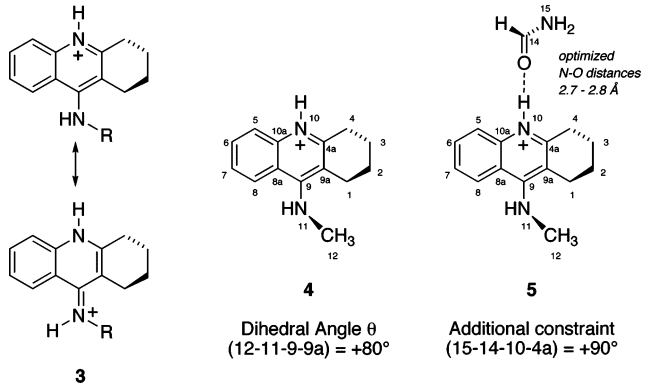


**Figure 9.** Resonance in protonated *N*-alkyltacrines **3** and designation of the dihedral angle in protonated *N*-methyltacrine **4** and its formamide complex **5**.

(Tyr334-Gly335 in *Tc*AChE) and the side-chain of Tyr337 (Phe330 in *Tc*AChE) adopt unexpected conformations in the complex.

**Orientation of the Alkylene Tether with Respect to the Tacrine Ring.** The endocyclic nitrogens of the catalytic-site tacrine units in the **2d** and **2f**/*Tc*AChE complexes are 2.9 and 3.0 Å, respectively, away from the carbonyl oxygen of His440. On the basis of these distances, it can be inferred that the tacrine moieties in the catalytic-site are protonated and donate a hydrogen bond to the His440 carbonyl oxygen. This is consistent with the fact that the conjugate acid of tacrine has a p$K_A$ of 9.8,[56] and such a hydrogen bonding interaction would contribute to ligand affinity. A protonated *N*-alkyl tacrine, **3**, would be expected to have maximal resonance stabilization if the *N*-alkyl substituent were roughly coplanar with the ring system (Figure 9).

An intermediate dihedral angle is seen for the catalytic tacrine unit in the **2d**/*Tc*AChE complex (dihedral angle = 135°, i.e., 45° out of coplanarity). However, for the catalytic tacrine unit of the **2f**/*Tc*AChE complex, a large deviation from coplanarity is seen (68°). It should be noted that in both cases, the fit of these carbon atoms was based on electron density considerations, and no restraints were placed on the coplanarity of the exocyclic nitrogen substituents. The final simulated annealing omit maps are also consistent with noncoplanarity of the exocyclic nitrogen substituent, and the B-factors of the linker carbon atoms are comparable to the exocyclic nitrogen. Attempts to impose coplanarity on the exocyclic nitrogen substituent caused distortion of the ring carbon C9, with little movement of the linker carbon atom (data not shown). So the conformation of the linker appears to be secure. These results are also consistent with the crystal structures of complexes with AChE of similar compounds (Table 4 and Figure 10).

To estimate the energetic penalty associated with these deviations from coplanarity, we performed density functional theory calculations (B3LYP/6-31G*//B3LYP/6-31G*)[57] on protonated *N*-methyl tacrine (**4**), determining optimized geometries as the dihedral angle $\theta$ was varied from 0 to 360° in 10° increments (see Supporting Information for computational details). These calculations estimate that the $\theta = 140°$ structure is only 1.5 kcal/mol above the global minimum, suggesting that the conformation adopted by the catalytic site tacrine in the **2d**/*Tc*AChE complex is low in energy. However, the adoption of a 70° dihedral angle by **4** puts it 7.2 kcal/mol higher than the global minimum. Thus, it appears that a significant energetic penalty is associated with the conformation of the catalytic site tacrine in the **2f**/*Tc*AChE complex. This energetic penalty is not significantly reduced at B3LYP/6-31+G*//B3LYP/6-31G*, and the explicit inclusion of a formamide moiety (Figure 9,

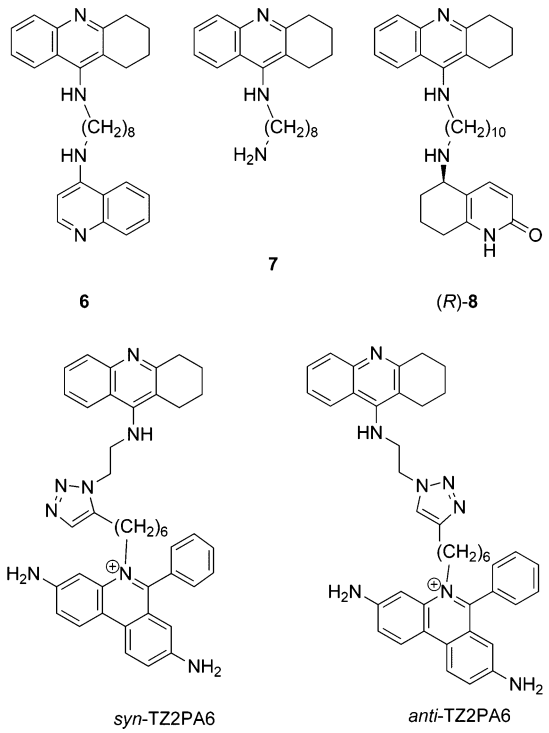


**Figure 10.** Structures of compounds compared in Table 4.

formamide complex **5**) to model the hydrogen bonding interaction with the His440 carbonyl reduces the penalty only slightly to 6.1 kcal/mol. A similar dihedral angle (73°) is observed for the presumably protonated peripheral site tacrine unit of the **2d**/*Tc*AChE complex. At this time, we are not able to account for these two unexpected dihedral angles in the tacrine dimer/*Tc*AChE complexes.

## Conclusions

In summary, we have shown that the structural basis for the observation that **2f** is an optimal inhibitor is that it forms favorable sandwich type stacking interactions in both the PAS and CAS with minimal protein rearrangement. **2d**, which is less potent, has only a one-sided stacking interaction in the peripheral site and induces a conformational change in the protein backbone near the acyl binding pocket. The structural changes to the native enzyme observed in the two complexes as well as other complexes discussed in the text, highlight the limitations of inhibitor design based on the structure of the native enzyme.

**Acknowledgment.** This study was supported by the European Commission Vth Framework Contracts QLK3-2000-00650 and QLG2-CT-2002-00988 (SPINE), the Minerva Foundation, the Kalman and Ida Wolens Foundation, the Jean and Jula Goldwurm Memorial Foundation, the Divadol Foundation, the Bruce Rosen Foundation, the Kimmelman Center for Biomolecular Structure and Assembly (Rehovot, Israel), and the Benoziyo Center for Neurosciences. We thank the staff at beamline ID14-2 at the ESRF in Grenoble for help with data collection. E.H.R. was supported by the Golda and Dr. Yehiel Shwartzman and Sara and Haim Medvedi Families Postdoctoral Fellowship. J.L.S. is the Morton and Gladys Pickman Professor of Structural Biology.

**Supporting Information Available:** (1) Details of computational chemistry methods; and (2) morphing movies of **2d**/*Tc*AChE and **2f**/*Tc*AChE, created with PyMol.[47] This material is available free of charge via the Internet at http://pubs.acs.org.

## References

(1) Drachman, D. A.; Leavitt, J. Human memory and the cholinergic system. *Arch. Neurol.* **1974**, *30*, 113−121.
(2) Bowen, D. M.; Allen, S. J.; Benton, J. S.; Goodhardt, M. J.; Haan, E. A.; Palmer, A. M.; Sims, N. R.; Smith, C. C.; Spillane, J. A.; Esiri, M. M.; Neary, D.; Snowdon, J. S.; Wilcock, G. K.; Davison, A. N. Biochemical assessment of serotonergic and cholinergic dysfunction and cerebral atrophy in Alzheimer's disease. *J. Neurochem.* **1983**, *41*, 266−272.
(3) Bartus, R. T.; Dean, R. L.; Beer, B.; Lippa, A. S. The cholinergic hypothesis of geriatric memory dysfunction. *Science* **1982**, *217*, 408−414.
(4) Dunnett, S. B.; Fibiger, H. C. Role of forebrain cholinergic systems in learning and memory: relevance to the cognitive deficits of aging and Alzheimer's dementia. *Prog. Brain Res.* **1993**, *98*, 413−420.
(5) Giacobini, E. Cholinesterase Inhibitors: From the Calabar Bean to Alzheimer Therapy. *Cholinestrases and Cholinesterase Inhibitors*; Martin Dunitz, Ltd.: London, 2000; pp 181−226.
(6) Greenblatt, H. M.; Dvir, H.; Silman, I.; Sussman, J. L. Acetylcholinesterase: A multifaceted target for structure-based drug design of anticholinesterase agents for the treatment of Alzheimer's disease. *J. Mol. Neurosci.* **2003**, *20*, 369−383.
(7) Nicolet, Y.; Lockridge, O.; Masson, P.; Fontecilla-Camps, J. C.; Nachon, F. Crystal structure of human butyrylcholinesterase and of its complexes with substrate and products. *J. Biol. Chem.* **2003**, *278*, 41141−41147.
(8) Perry, E. K.; Perry, R. H.; Blessed, G.; Tomlinson, B. E. Changes in brain cholinesterases in senile dementia of Alzheimer type. *Neuropathol. Appl. Neurobiol.* **1978**, *4*, 273−277.
(9) Giacobini, E. Cholinesterase inhibitors: new roles and therapeutic alternatives. *Pharmacol. Res.* **2004**, *50*, 433−440.
(10) Tasker, A.; Perry, E. K.; Ballard, C. G. Butyrylcholinesterase: impact on symptoms and progression of cognitive impairment. *Expert. Rev. Neurother.* **2005**, *5*, 101−106.
(11) Inestrosa, N. C.; Alvarez, A.; Perez, C. A.; Moreno, R. D.; Vicente, M.; Linker, C.; Casanueva, O. I.; Soto, C.; Garrido, J. Acetylcholinesterase accelerates assembly of amyloid-beta-peptides into Alzheimer's fibrils: possible role of the peripheral site of the enzyme. *Neuron* **1996**, *16*, 881−891.
(12) Reyes, A. E.; Perez, D. R.; Alvarez, A.; Garrido, J.; Gentry, M. K.; Doctor, B. P.; Inestrosa, N. C. A monoclonal antibody against acetylcholinesterase inhibits the formation of amyloid fibrils induced by the enzyme. *Biochem. Biophys. Res. Commun.* **1997**, *232*, 652−655.
(13) Bartolini, M.; Bertucci, C.; Cavrini, V.; Andrisano, V. beta-Amyloid aggregation induced by human acetylcholinesterase: inhibition studies. *Biochem. Pharmacol.* **2003**, *65*, 407−416.
(14) De Ferrari, G. V.; Canales, M. A.; Shin, I.; Weiner, L. M.; Silman, I.; Inestrosa, N. C. A structural motif of acetylcholinesterase that promotes amyloid beta-peptide fibril formation. *Biochemistry* **2001**, *40*, 10447−10457.
(15) Olivera-Bravo, S.; Ivorra, I.; Morales, A. The acetylcholinesterase inhibitor BW284c51 is a potent blocker of Torpedo nicotinic AChRs incorporated into the Xenopus oocyte membrane. *Br. J. Pharmacol.* **2005**, *144*, 88−97.
(16) Li, W.; Pi, R.; Chan, H. H.; Fu, H.; Lee, N. T.; Tsang, H. W.; Pu, Y.; Chang, D. C.; Li, C.; Luo, J.; Xiong, K.; Li, Z.; Xue, H.; Carlier, P. R.; Pang, Y.; Tsim, K. W.; Li, M.; Han, Y. Novel dimeric acetylcholinesterase inhibitor bis(7)-tacrine, but not donepezil, prevents glutamate-induced neuronal apoptosis by blocking *N*-methyl-D-aspartate receptors. *J. Biol. Chem.* **2005**, *280*, 18179−18188.
(17) Piazzi, L.; Rampa, A.; Bisi, A.; Gobbi, S.; Belluti, F.; Cavalli, A.; Bartolini, M.; Andrisano, V.; Valenti, P.; Recanatini, M. 3-(4-[[Benzyl(methyl)amino]methyl]phenyl)-6,7-dimethoxy-2H-2-chromenone (AP2238) inhibits both acetylcholinesterase and acetylcholinesterase-induced beta-amyloid aggregation: a dual function lead for Alzheimer's disease therapy. *J. Med. Chem.* **2003**, *46*, 2279−2282.
(18) Campiani, G.; Fattorusso, C.; Butini, S.; Gaeta, A.; Agnusdei, M.; Gemma, S.; Persico, M.; Catalanotti, B.; Savini, L.; Nacci, V.; Novellino, E.; Holloway, H. W.; Greig, N. H.; Belinskaya, T.; Fedorko, J. M.; Saxena, A. Development of molecular probes for the identification of extra interaction sites in the mid-gorge and peripheral sites of butyrylcholinesterase (BuChE). Rational design of novel, selective, and highly potent BuChE inhibitors. *J. Med. Chem.* **2005**, *48*, 1919−1929.
(19) Luo, W.; Yu, Q. S.; Zhan, M.; Parrish, D.; Deschamps, J. R.; Kulkarni, S. S.; Holloway, H. W.; Alley, G. M.; Lahiri, D. K.; Brossi, A.; Greig, N. H. Novel anticholinesterases based on the molecular skeletons of furobenzofuran and methanobenzodioxepine. *J. Med. Chem.* **2005**, *48*, 986−994.

(20) Rosini, M.; Andrisano, V.; Bartolini, M.; Bolognesi, M. L.; Hrelia, P.; Minarini, A.; Tarozzi, A.; Melchiorre, C. Rational approach to discover multipotent anti-Alzheimer drugs. *J. Med. Chem.* **2005**, *48*, 360−363.
(21) Jencks, W. P. Binding energy, specificity, and enzymic catalysis: the circe effect. *Adv. Enzymol. Relat. Areas Mol. Biol.* **1975**, *43*, 219−410.
(22) Sussman, J. L.; Harel, M.; Frolow, F.; Oefner, C.; Goldman, A.; Toker, L.; Silman, I. Atomic structure of acetylcholinesterase from *Torpedo californica*: a prototypic acetylcholine-binding protein. *Science* **1991**, *253*, 872−879.
(23) Silman, I.; Sussman, J. L. Acetylcholinesterase: 'classical' and 'non-classical' functions and pharmacology. *Curr. Opin. Pharmacol.* **2005**, *5*, 293−302.
(24) Bergmann, F.; Wilson, I. B.; Nachmansohn, D. The inhibitory effect of stilbamidine, curare and related compounds and its relationship to the active groups of acetylcholine esterase. Action of stilbamidine upon nerve impulse conduction. *Biochim. Biophys. Acta* **1950**, *6*, 217−224.
(25) Austin, L.; Berry, W. K. Two Selective inhibitors of cholinesterase. *Biochem. J.* **1953**, *54*, 695−700.
(26) Hodge, A. S.; Humphrey, D. R.; Rosenberry, T. L. Ambenonium is a rapidly reversible noncovalent inhibitor of acetylcholinesterase, with one of the highest known affinities. *Mol. Pharmacol.* **1992**, *41*, 937−942.
(27) Pang, Y.-P.; Quiram, P.; Jelacic, T.; Hong, F.; Brimijoin, S. Highly potent, selective, and low cost bis-tetrahydroaminacrine inhibitors of acetylcholinesterase. *J. Biol. Chem.* **1996**, *271*, 23646−23649.
(28) Lewis, W. G.; Green, L. G.; Grynszpan, F.; Radic, Z.; Carlier, P. R.; Taylor, P.; Finn, M. G.; Sharpless, K. B. Click chemistry in situ: acetylcholinesterase as a reaction vessel for the selective assembly of a femtomolar inhibitor from an array of building blocks. *Angew. Chem., Int. Ed.* **2002**, *41*, 1053−1057.
(29) Krasinski, A.; Radic, Z.; Manetsch, R.; Raushel, J.; Taylor, P.; Sharpless, K. B.; Kolb, H. C. In situ selection of lead compounds by click chemistry: target-guided optimization of acetylcholinesterase inhibitors. *J. Am. Chem. Soc.* **2005**, *127*, 6686−6692.
(30) Du, D. M.; Carlier, P. R. Development of bivalent acetylcholinesterase inhibitors as potential therapeutic drugs for Alzheimer's disease. *Curr. Pharm. Des.* **2004**, *10*, 3141−3156.
(31) Carlier, P. R.; Chow, E. S.; Han, Y.; Liu, J.; El Yazal, J.; Pang, Y. P. Heterodimeric tacrine-based acetylcholinesterase inhibitors: investigating ligand-peripheral site interactions. *J. Med. Chem.* **1999**, *42*, 4225−4231.
(32) Harel, M.; Sussman, J. L.; Krejci, E.; Bon, S.; Chanal, P.; Massoulié, J.; Silman, I. Conversion of acetylcholinesterase to butyrylcholinesterase: modeling and mutagenesis. *Proc. Natl Acad. Sci. U.S.A.* **1992**, *89*, 10827−10831.
(33) Farlow, M.; Gracon, S. I.; Hershey, L. A.; Lewis, K. W.; Sadowsky, C. H.; Dolan-Ureno, J. A controlled trial of tacrine in Alzheimer's disease. The Tacrine Study Group. *Jama* **1992**, *268*, 2523−2529.
(34) Watkins, P. B.; Zimmerman, H. J.; Knapp, M. J.; Gracon, S. I.; Lewis, K. W. Hepatotoxic effects of tacrine administration in patients with Alzheimer's disease. *JAMA* **1994**, *271*, 992−998.
(35) Pang, Y.-P.; Kozikowski, A. Prediction of the binding sites of huperzine A in acetylcholinesterase by docking studies. *J. Comput-Aided Mol. Des.* **1994**, *8*, 669−681.
(36) Harel, M.; Schalk, I.; Ehret-Sabatier, L.; Bouet, F.; Goeldner, M.; Hirth, C.; Axelsen, P.; Silman, I.; Sussman, J. L. Quaternary ligand binding to aromatic residues in the active-site gorge of acetylcholinesterase. *Proc. Natl Acad. Sci. U.S.A.* **1993**, *90*, 9031−9035.
(37) Carlier, P. R.; Han, Y. F.; Chow, E. S.; Li, C. P.; Wang, H.; Lieu, T. X.; Wong, H. S.; Pang, Y. P. Evaluation of short-tether bis-THA AChE inhibitors. A further test of the dual binding site hypothesis. *Bioorg. Med. Chem.* **1999**, *7*, 351−357.
(38) Ravelli, R. B. G.; Sweet, R. M.; Skinner, J. M.; Duisenberg, A. J. M.; Kroon, J. STRATEGY: a program to optimize the starting spindle angle and scan range for X-ray data collection. *J. Appl. Crystallogr.* **1997**, *30*, 551−554.
(39) Otwinowski, Z.; Minor, W. Processing of X-ray diffraction data collected in oscillation mode. *Methods Enzymol.* **1997**, *276*, 307−326.
(40) Collaborative Computational Project Number 4 The CCP4 Suite: Programs for Protein Crystallography. *Acta Crystallogr., Sect D* **1994**, *50*, 760−763.
(41) French, S.; Wilson, K. On Treatment of Negative Intensity Observations. *Acta Crystallogr., Sect A* **1978**, *34*, 517−525.
(42) Brunger, A. T. Free R Value: Cross-Validation in Crystallography. *Methods Enzymol.* **1997**, *277*, 366−396.
(43) Brunger, A. T.; Adams, P. D.; Clore, G. M.; DeLano, W. L.; Gros, P.; Grosse-Kunstleve, R. W.; Jiang, J. S.; Kuszewski, J.; Nilges, M.; Pannu, N. S.; Read, R. J.; Rice, L. M.; Simonson, T.; Warren, G. L. Crystallography & NMR system: A new software suite for macromolecular structure determination. *Acta Crystallogr., Sect D* **1998**, *54*, 905−921.
(44) McRee, D. E. XtalView/Xfit- -A versatile program for manipulating atomic coordinates and electron density. *J. Struct. Biol.* **1999**, *125*, 156−165.
(45) Brünger, A. T.; Rice, L. M. Crystallographic refinement by simulated annealing: methods and applications. *Methods Enzymol.* **1997**, *277*, 234−269.
(46) Merritt, E. A.; Bacon, D. J. Raster3D: photorealistic molecular graphics. *Methods Enzymol.* **1997**, *277*, 505−524.
(47) DeLano, W. L. *The PyMOL Molecular Graphics System*; DeLano Scientific: San Carlos, CA.
(48) Morel, N.; Bon, S.; Greenblatt, H. M.; Van Belle, D.; Wodak, S. J.; Sussman, J. L.; Massoulie, J.; Silman, I. Effect of mutations within the peripheral anionic site on the stability of acetylcholinesterase. *Mol. Pharmacol.* **1999**, *55*, 982−992.
(49) Philippsen, A. *DINO*: Visualizing Structural Biology.
(50) Boehr, D. D.; Farley, A. R.; Wright, G. D.; Cox, J. R. Analysis of the pi-pi stacking interactions between the aminoglycoside antibiotic kinase APH(3′)-IIIa and its nucleotide ligands. *Chem. Biol.* **2002**, *9*, 1209−1217.
(51) Colletier, J. P.; Sanson, B.; Nachon, F.; Gabellieri, E.; Fattorusso, C.; Campiani, G.; Weik, M. Conformational flexibility in the peripheral site of *Torpedo californica* acetylcholinesterase revealed by the complex structure with a bifunctional inhibitor. *J. Am. Chem. Soc.* **2006**, *128*, 4526−4527.
(52) Millard, C. B.; Kryger, G.; Ordentlich, A.; Harel, M.; Raves, M.; Greenblatt, H. M.; Segall, Y.; Barak, D.; Shafferman, A.; Silman, I.; Sussman, J. L. Crystal structure of "aged" phosphylated *Torpedo* acetylcholinesterase: nerve agent reaction products at the atomic level. *Biochemistry* **1999**, *38*, 7032−7039.
(53) Greenblatt, H. M.; Guillou, C.; Guenard, D.; Argaman, A.; Botti, S.; Badet, B.; Thal, C.; Silman, I.; Sussman, J. L. The complex of a bivalent derivative of galanthamine with torpedo acetylcholinesterase displays drastic deformation of the active-site gorge: implications for structure-based drug design. *J. Am. Chem. Soc.* **2004**, *126*, 15405−15411.
(54) Greenblatt, H. M.; Kryger, G.; Lewis, T.; Silman, I.; Sussman, J. Structure of acetylcholinesterase complexed with (−)-galanthamine at 2.3 Å resolution. *FEBS Lett.* **1999**, *463*, 321−326.
(55) Bourne, Y.; Kolb, H. C.; Radic, Z.; Sharpless, K. B.; Taylor, P.; Marchot, P. Freeze-frame inhibitor captures acetylcholinesterase in a unique conformation. *Proc. Natl. Acad. Sci. U.S.A.* **2004**, *101*, 1449−1454.
(56) Desai, M. C.; Thadeio, P. F.; Lipinski, C. A.; Liston, D. R.; Spencer, R. W.; Williams, I. H. Physical parameters for brain uptake: optimizing log P, log D, and p$K_a$ of THA. *Bioorg. Med. Chem. Lett.* **1991**, *1*, 411−414.
(57) Frisch, M. J.; Trucks, G. W.; Schlegel, H. B.; Scuseria, G. E.; Robb, M. A.; Cheeseman, J. R.; Montgomery, J. A., Jr.; Vreven, T.; Kudin, K. N.; Burant, J. C.; Millam, J. M.; Iyengar, S. S.; Tomasi, J.; Barone, V.; Mennucci, B.; Cossi, M.; Scalmani, G.; Rega, N.; Petersson, G. A.; Nakatsuji, H.; Hada, M.; Ehara, M.; Toyota, K.; Fukuda, R.; Hasegawa, J.; Ishida, M.; Nakajima, T.; Honda, Y.; Kitao, O.; Nakai, H.; Klene, M.; Li, X.; Knox, J. E.; Hratchian, H. P.; Cross, J. B.; Bakken, V.; Adamo, C.; Jaramillo, J.; Gomperts, R.; Stratmann, R. E.; Yazyev, O.; Austin, A. J.; Cammi, R.; Pomelli, C.; Ochterski, J. W.; Ayala, P. Y.; Morokuma, K.; Voth, G. A.; Salvador, P.; Dannenberg, J. J.; Zakrzewski, V. G.; Dapprich, S.; Daniels, A. D.; Strain, M. C.; Farkas, O.; Malick, D. K.; Rabuck, A. D.; Raghavachari, K.; Foresman, J. B.; Ortiz, J. V.; Cui, Q.; Baboul, A. G.; Clifford, S.; Cioslowski, J.; Stefanov, B. B.; Liu, G.; Liashenko, A.; Piskorz, P.; Komaromi, I.; Martin, R. L.; Fox, D. J.; Keith, T.; Al-Laham, M. A.; Peng, C. Y.; Nanayakkara, A.; Challacombe, M.; Gill, P. M. W.; Johnson, B.; Chen, W.; Wong, M. W.; Gonzalez, C.; Pople, J. A. *Gaussian 03*, revision C.02; Gaussian, Inc.: Wallingford, CT, 2004.
(58) Haviv, H.; Wong, D. M.; Greenblatt, H. M.; Carlier, P. R.; Pang, Y. P.; Silman, I.; Sussman, J. L. Crystal packing mediates enantioselective ligand recognition at the peripheral site of acetylcholinesterase. *J. Am. Chem. Soc.* **2005**, *127*, 11029−11036.

JM060164B